Condition Monitoring Algorithm for Piezoresistive Silicon-Based Stress Sensor Data Obtained from Electronic Control Units

Prisacaru, Alexandru; Palczynska, Alicja; Gromala, Przemyslaw Jakub; Han, Bongtae; Zhang, Guo Qi

DOI
10.1109/ECTC.2017.73

Publication date
2017

Document Version
Accepted author manuscript

Published in
Proceedings - IEEE 67th Electronic Components and Technology Conference, ECTC 2017

Citation (APA)
Prisacaru, A., Palczynska, A., Gromala, P. J., Han, B., & Zhang, G. Q. (2017). Condition Monitoring Algorithm for Piezoresistive Silicon-Based Stress Sensor Data Obtained from Electronic Control Units. In *Proceedings - IEEE 67th Electronic Components and Technology Conference, ECTC 2017* (pp. 1119-1127). Article 7999824 IEEE. https://doi.org/10.1109/ECTC.2017.73

Condition Monitoring Algorithm for Piezoresistive Silicon-based Stress Sensor Data Obtained from Electronic Control Units

Alexandru Prisacaru, Alicja Palczynska, Przemyslaw Gromala
Automotive Electronics
Robert Bosch GmbH
Reutlingen, Germany
e-mail: Alexandru.Prisacaru@de.bosch.com, Alicja.Palczynska@de.bosch.com, PrzemyslawJakub.Gromala@de.bosch.com

Bongtae Han
Mechanical Engineering Department
University of Maryland College Park
MD 20742, USA
e-mail: bthan@umd.edu,

Guo Qi Zhang
Microelectronics Department,
Delft University of Technology
Delft, 2600, Netherlands
e-mail: G.Q.Zhang@tudelft.nl

***Abstract* — Recent advancements in automotive technologies, most notably autonomous driving, demand electronic systems much more complex than realized in the past. The automotive industry has been forced to adopt advanced consumer electronics to satisfy the demand, and thus it becomes more challenging to assess system reliability while adopting the new technologies. The system level reliability can be enforced by implementing a process called condition monitoring. In this paper, a piezoresistive silicon based stress sensor is implemented to detect physical damages in outer molded electronic control units (ECU) subjected to reliability testing conditions. The test vehicle consists of six DPAK power packages and three stress sensors mounted on a Printed Circuit Board (PCB). A unique algorithm is proposed and implemented to handle the data obtained from the piezoresistive stress sensing cells. The accuracy of measured data is examined by Finite Element method (FEM), and the physical changes are validated with Scanning Acoustic Microscope (SAM).**

Keywords - Condition Monitoring, Stress Sensor, Electronic Control Units, Fault Detection

I. INTRODUCTION

Condition Monitoring (CM) is a process to monitor parameters of system conditions, which is a critical component in predictive maintenance. Condition monitoring techniques have been used extensively for large-scale machineries and structures. More recently, condition monitoring has been adopted for advanced electronic systems, most notably, automotive electronics including batteries.

Conventional sensors (e.g., sensors for temperature, humidity, vibration, etc.) are not most adequate for the condition monitoring of complex electronic system as they only measure the loading conditions. The piezoresistive stress sensors were developed to cope with the problem. The sensor measures directly the stresses of a silicon chip, and it was utilized in several electronic packaging applications [1][2][3][4][5][6][7][8][11]. It was also implemented successfully to monitor the stresses in advanced electronic control unit (ECU) subjected to reliability testing conditions [9][10].

In order to extend its applicability into the Prognostics and Health Management (PHM) domain, it is required to link the measured stress to the damage or fault of the ECU, as illustrated in Figure 1. The objective of this paper is, thus, to propose special algorithms to handle the stress sensor data obtained from the ECU. The proposed algorithms are presented after briefly describing the sensor. The implementation results are followed using the data obtained from a test vehicle.

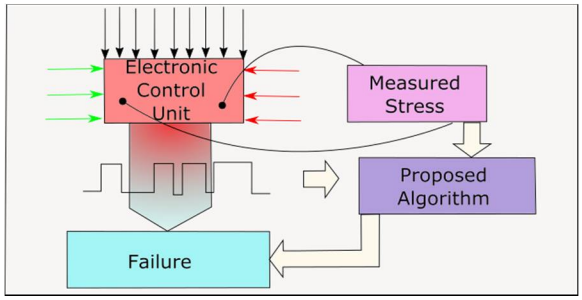

Figure 1. Stress Failure relationship. Various type of loads are causing ECU failures. The proposed algorithm is linking the measured stress with the failure.

II. IFORCE SENSOR

The working principle of the piezoresistive silicon based stress sensor can be found in Refs. [1] and [12]. A land grid array (LGA) package used in this study is shown in Figure 2. It is a standard sensor package, which contains a pair of symmetrically located sensor with 12 sensing cells. Every cell is capable of measuring the in-plane shear stress, σ_{xy}, and the difference of in-plane normal stress components, $D(\sigma) = \sigma_{xx} - \sigma_{yy}$.

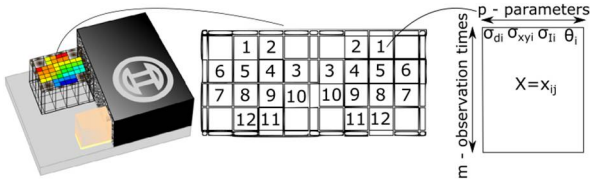

Figure 2. Sensor cell numbering position and the acquired data.

The relationship between the measured currents and the stresses are:

$$\sigma_{xx} - \sigma_{yy} = \frac{1}{\pi_{44}^{p}} \frac{I_{OUT} - I_{IN}}{I_{OUT} + I_{IN}} \quad (1)$$

$$\sigma_{xy} = \frac{1}{\pi_{11}^{n} - \pi_{12}^{n}} \frac{I_{OUT} - I_{IN}}{I_{OUT} + I_{IN}} \quad (2)$$

where π_{11}, π_{12}, π_{44} are the piezoresistive coefficients of silicon; and I_{IN}, I_{OUT} are the currents measured at the input and output of the sensor, respectively.

The stresses can be used to produce the maximum shear stress and the angle of principal stresses as:

$$\tau_{max} = \frac{\sigma_1 - \sigma_2}{2} = \sqrt{\left(\frac{\sigma_{xx} - \sigma_{yy}}{2}\right)^2 + \tau_{xy}^2} \quad (3)$$

$$\tan 2\theta_p = \frac{2\tau_{xy}}{\sigma_{xx} - \sigma_{yy}} \quad (4)$$

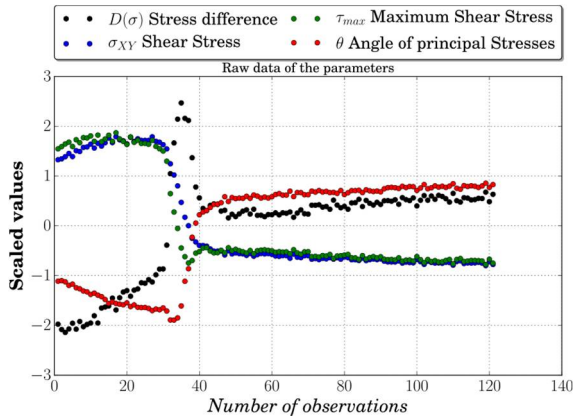

Figure 3. Raw data example at room temperature during delamination.

Representative raw data, two measured parameters and two calculated parameters are shown in Figure 3. The data was collected from one cell during failure propagation.

The parameter relationship it is captured in a 2D Mohr Circle as depicted in Figure 4. Also, this description can capture all the parameters in one circle.

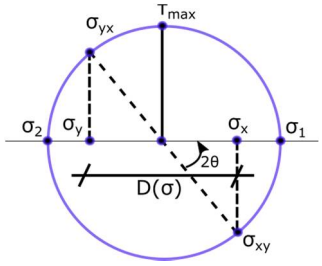

Figure 4. 2D Mohr Cicle. Describes the relationship between parameters.

III. PROPOSED ALGORITHM

A typical health dataset, *X*, contains *m* rows and *p* columns, where *m* is the total number of observations before observing any anomalies and *p* the total number of the performance parameters. Each sensor output having 12 cells and 4 parameters can have up to 48 performance parameters.

The first part of the algorithm starts with extracting and creating an initial healthy baseline, and subsequently assessing the health at every measurement step. If no deviations are detected at that particular data point in time, the healthy baseline is updated as shown in Figure 5.

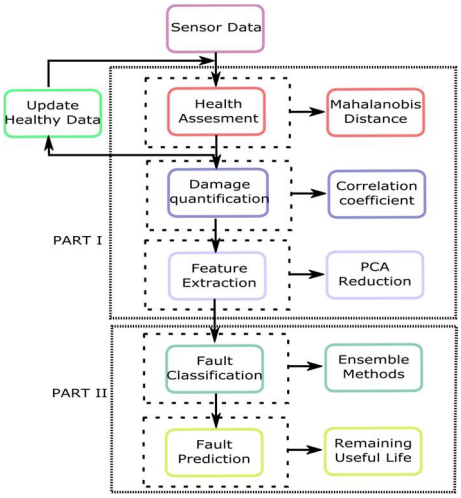

Figure 5. Algorithm flowchart.

In this study, Mahalanobis Distance (MD) [9][13] is employed to assess the health or to detect any anomalies. It is also called quadratic distance as it can measure the difference between two sets of data as well as the distance between a point and a set of data. Although effective, it could detect false signals (e.g., outliers, changes not associated with damage, etc.). An additional step that quantifies the damage is added to avoid false detection. Let's assume that an anomaly is detected at the *n*th observation. To assure that this detection point is not an outlier, another set of measurement should be conducted at $n + h$, where h depends on the number of performance parameters. A new dataset, *Y*, is created, containing h rows and p columns. On this newly created dataset h by p, a correlation matrix is constructed. This correlation matrix is assumed to be the failure correlation matrix, and it is compared with the healthy baseline correlation matrix used in MD method. This is possible with Fisher *r-to-z*

transformation [14], which assess the significance of the difference between two correlation coefficients.

In case that the significance of the difference is close to zero it means that the probability of two sets to be similar is very high. If the *z* value is around one the probability that these datasets to be similar is less than 0.05. This additional step is checking if the data points are outliers and it can quantify the damage by estimating the *z*-scores of the performance parameters.

As last step PCA is used for the data reduction to facilitate cheaper and faster transmission [15]. This last step is performed only if MD detects any anomaly and if the significance of the difference between two correlation coefficients is at least equal to one. In this way it is certain that the detection point is not an outlier, but an entire dataset different from the healthy baseline.

IV. IMPLEMENTATION

A. *Test vehicle*

The test vehicle used in the study is shown in Figure 6. It consists of six DPAK's and three stress sensors mounted on the top and bottom sides of a PCB. This assembly was molded by an injection molding process. The location of the sensors was chosen to capture the maximum stress. Every sensor package contains 2 symmetrical sensors. Their locations and their arbitrary numbering is presented in Figure 6.

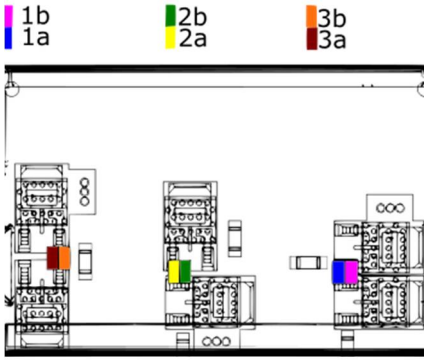

Figure 6. The position of each sensor on the Outer molded electronic control unit.

The study was performed on 10 samples, but the results are shown from the most significant 2 samples considering the large amount of data.

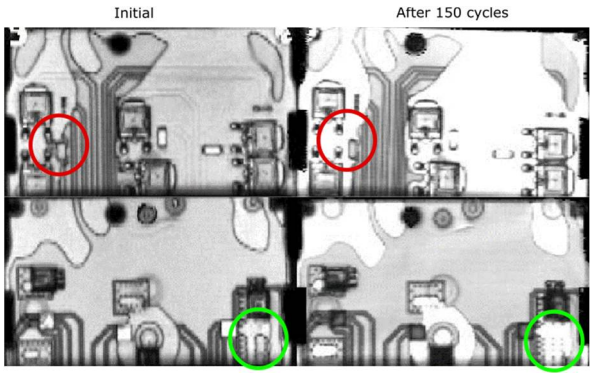

a)

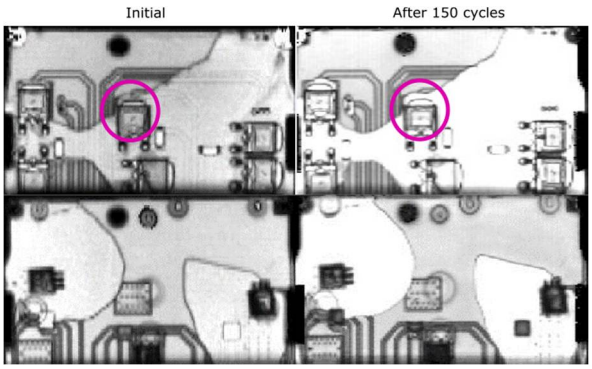

b)

Figure 7. a) Sample 1 SAM images of the initial delamination and the delamination propagation after 150 cycles. The red and green circles represent the area where there are changes in the delamination area. b) Sample 2 SAM images of the initial delamination and the delamination propagation after 150 cycles. The magenta circles represent the area where there are changes in the delamination area.

Some initial delamination was created on the samples before the injection molding process. The delamination areas are visible in the initial SAM images as shown in Figure 7. The locations of delamination are randomly distributed. It is observed that the delamination is present in the vicinity of sensor 3 in both sides of the PCB of Sample 2. Thus, it is expected that the most damage should be recorded by sensor 3a, 3b of Sample 2.

The delamination is represented by the area in lighter color and the lack of visibility of the circuit board footprint, as shown in Figure 7.

B. *Initial Data*

Data was recorded through an acquisition system during the experiments. The samples were placed in a temperature chamber, and they were exposed to a passive cycling loading condition of -40° C to 125° C with a dwelling time of 15 minutes. The dwelling time was predetermined to provide a condition where all components reach the uniform distribution at target temperatures. SAM images of the samples were recorded before and after each 150 cycle.

The sensor signal was investigated by a predictive FEM model. The geometry and the loading conditions are identical to the experiment. The process to validate the model can be found in Ref. [16].

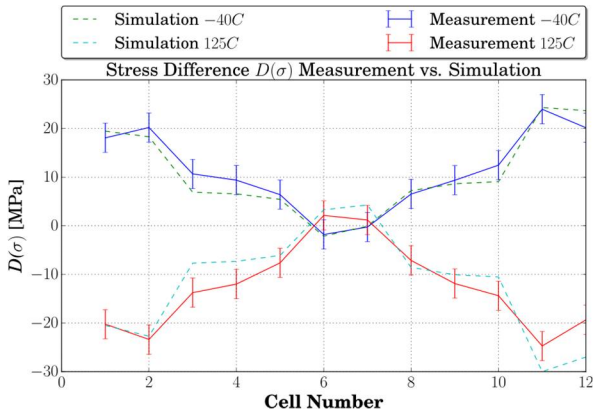

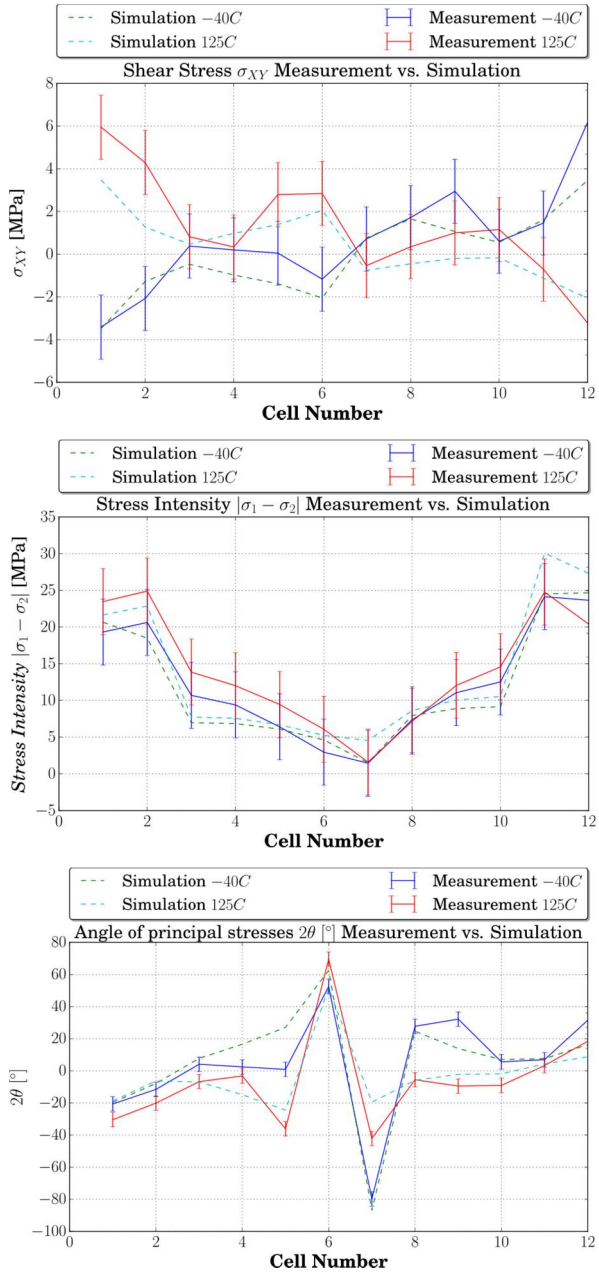

Figure 8. FEM examination of the test vehicle.

The modelling predictions are compared with the experimental data in Figure 8. The results show very good agreement. The small deviations are attributed to the uncertainties of the stress sensor [17] and the material properties used in the simulation.

The repeatability of measurements is known to be 0.3 MPa, and sample-to-sample variations are 2 – 6 MPa. From these graphs it is identified the sensitivity of each cell in the healthy stress state. It is clear that from all the parameters, cell 1, 2, 11 and 12 have the highest deviation between different loading conditions. This means that the higher stress state is located at the outer areas of the chip. This observation is important for further development of the stress sensor and also for data reduction strategies.

The simulation data is used to examine the measurements. It also provides better understanding about the mechanical processes and ultimately help develop a prognostics physical model. It can be further used for model-based fault detection by considering the residuals, which can be utilized to classify different failure modes behavior.

C. *Data from Thermal Cycling Data*

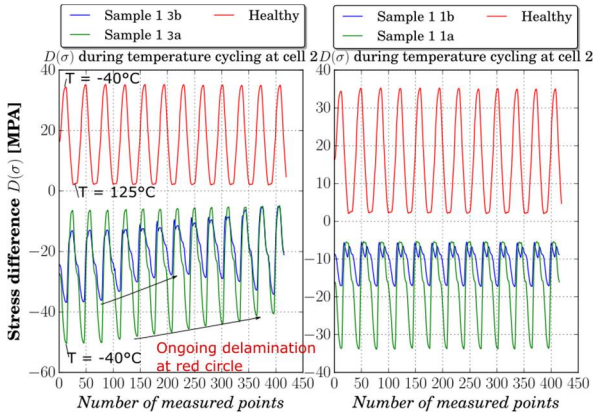

Figure 9. Comparison between measured stress difference for healthy and delaminated sample. The stress state represent the absolute values of stress, hence it contains also the residual stresses from manufacturing.

Between the first and the 50th cycle, changes in the stress difference and shear stress were observed. Some of these changes are recorded around 50th cycle, and the results are depicted in Figure 9. There are changes in stress difference in both sensors 3a and 3b from Sample 1. The sample and the red circle corresponding to the delamination propagation can be visualized in Figure 7.

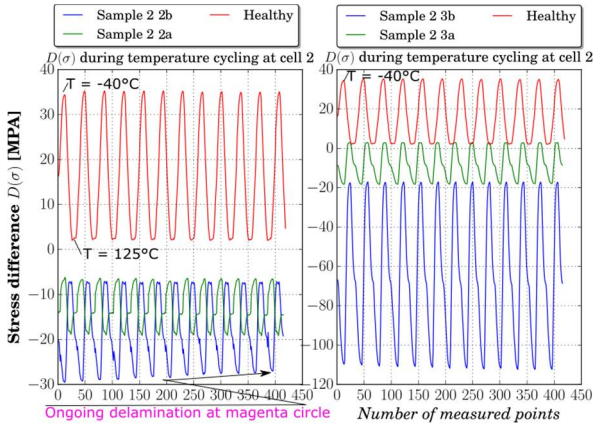

Figure 10. Comparison between measured stress difference for healthy and delaminated samples. On the blue line representing the Sample 2 Sensor 2b it is noticed an increasing in stress difference during temperature cycling corresponding to the delamination of the magenta circle in Figure 7. a).

From the same interval of cycles it can also be observed a change in difference of stress for sensor 2b from Sample 2 as depicted in Figure 10. The sample and the magenta circle representing the delamination propagation can be visualized in Figure 7.

The corresponding shear stress from the interval of cycles described above it can also be observed a change for sensor 3b and 3a from Sample 1 as depicted in Figure 10. The sample and the red circle representing the delamination propagation can be visualized in Figure 7.

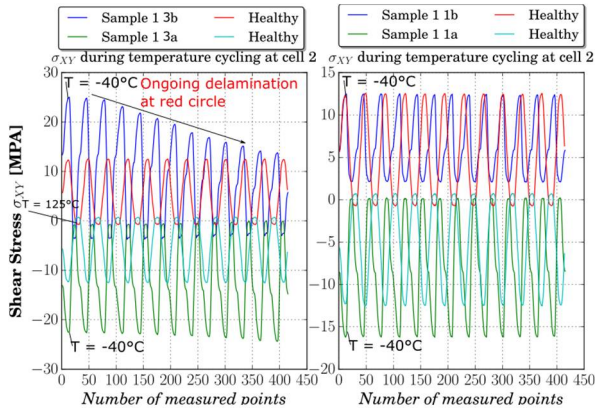

Figure 11. Comparison between measured shear stress for healthy and delaminated samples. On the blue line representing the Sample 1 Sensor 3b it is noticed a decreasing in shear stress during temperature cycling corresponding to the delamination of the red circle in Figure 7. a).

Due to the complexity of the structure and the big amount of data, it is challenging to interpret the data quantitatively. Several algorithms such as statistical pattern recognition methods and machine learning are considered to interpret the data.

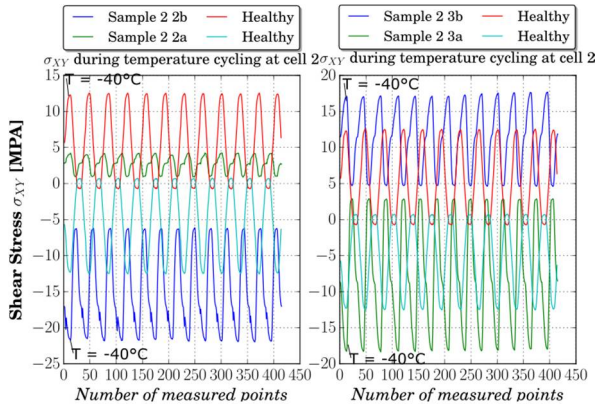

Figure 12. Comparison between measured shear stress for healthy and delaminated samples.

The corresponding shear stress of the Sample 2 is depicted in Figure 12. In the case of Sample 1 there were changes on both components of stress, but in this case there are changes only in the stress difference component.

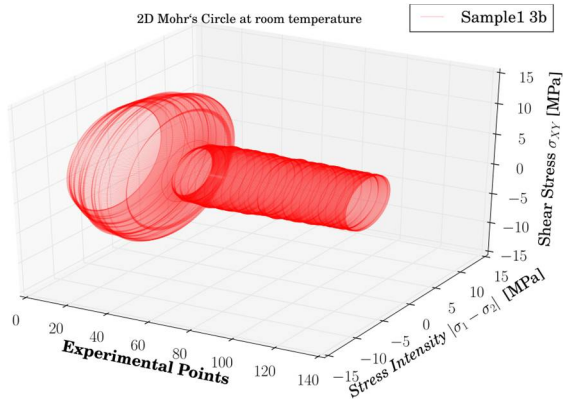

Figure 13. This is a representation of the 2D Mohr`s Circle of the data acquired during the experiments at cell 2 Sensor 3b Sample 1 during delamination.

In order to capture both parameters in one graph, Mohr's circles were plotted during the delamination. The results are shown in Figure 13, where the radius and the diameter represent the maximum shear stress and the difference of the principal stresses, respectively.

It is clear from Figure 13 that the diameter increases first and decreases rapidly after approximately 30 cycles. It is speculated that energy release associated with crack propagation may be attributed to the diameter reduction.

At low temperatures, the stress state is higher because of the large ΔT from the stress free point temperature. Therefore, any change in stress state can be more visible. In addition, the brittle behavior at low temperatures can accelerate the delamination.

D. Failure Analysis by SAM

As shown in Figure 7, changes in the delamination area were observed after 150 cycles. The pictures shown reveals two important properties which should be found in the data as well. The first property is represented by the fact that the samples contain an a priori delamination and the second property by the change in the delamination area due to the damage progress.

These properties have correspondence in the data by the stress value differences from the healthy samples and by the ongoing stress change after the cycle 35-50.

E. Data Analysis by the Proposed Algorithm

1) Health Assessment

For computing MD, the sets of compared data do not need to have the same amount of rows. In this study rows refers to the number of observations and creates the possibility to compare the healthy dataset with just one failure measurement point. This is convenient in health monitoring, considering that many other methods require a certain amount of observation points.

In this approach a healthy baseline and a threshold are needed to classify the product states (healthy or unhealthy). Several steps are required to calculate MD as follows:

- Step 1. Calculate the average of each column:

$$\bar{x}_i = \frac{1}{m}\sum_{j=1}^{m} x_{ij} \tag{5}$$

- Step 2. Calculate the standard deviation

$$s_i = \sqrt{\frac{\sum_{j=1}^{m}(x_{ij} - \bar{x}_i)^2}{m-1}} \tag{6}$$

- Step 3. Normalize the values

$$z_{ij} = \frac{x_{ij} - \bar{x}_i}{s_i} \tag{7}$$

- Step 4. Correlation matrix

$$C = \frac{1}{m-1}\sum_{j=1}^{m} Z_j Z_j^T \tag{8}$$

- Step 5. Mahalanobis Distance

$$MD_j = \frac{1}{p} Z_j^T C^{-1} Z_j \tag{9}$$

The next step is to add the normalized values of the next measurement and to compute the MD keeping the same correlation matrix from the healthy baseline. If the measurement point does not exceed the threshold, it is added to the healthy correlation matrix.

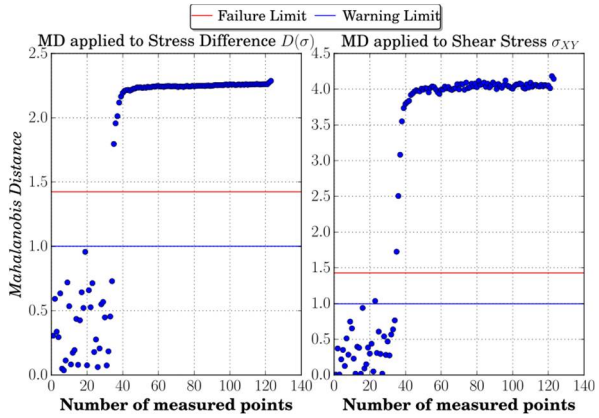

Figure 14. Mahalanobis Distance calculated over the 12 cells of the Sample 1 S3b. The healthy base is established on the first measurements and every point in measurement is calculated. In this graph there is changes due to the delamination showed in Figure 7.a).

For threshold determination, a probabilistic approach is used. Since the MD are not normally distributed, a Box-Cox transformation [18] is used to convert the data into a normal distribution. A warning limit threshold is defined as *(μ+2σ)* and a fault alarm threshold as *(μ+3σ)*, based on the normal distribution parameters.

The healthy baseline should have more rows than columns, considering that the rows represents the number of measurements and columns the number of parameters. For assuring good results, it is recommended that the ratio *m/p* should be as high as possible, otherwise the outliers can shift the sample mean and inflate the correlation matrix [19].

A representative MD for both stress components is shown in Figure 14. The healthy baseline is created on the first 35 measurement points. The data points exceeding the failure limit are clearly seen in the MD results. The incidents are expected from the raw data (Figure 11), but the MD results provide a more definitive health state of the specimen through the multi-variate to uni-variate conversion.

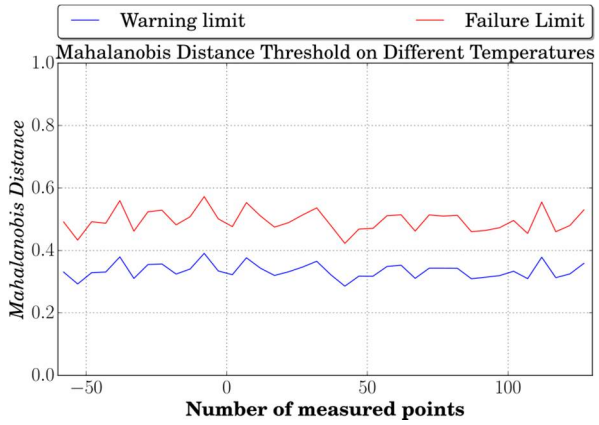

Figure 15. Threshold Evaluation performed at all temperatures.

The threshold at different temperatures is computed from the healthy data (i.e., no initial delamination), and the result is plotted in Figure 15. It is evident that the threshold does not change with the temperature, which implies that the healthy baseline can be created at any temperature.

MD method is preferred for fault/anomaly detection because of its advantages related to the requirements in health monitoring; they include fast calculation, no failure data requires, single measurement point required and temperature independent threshold.

2) Damage Quantification

This step is necessary to overcome the possibility of detecting outliers or changes in stress values which are not associated with any damage.

In this subsection, the correlation matrix of the healthy baseline without initial delamination is compared with the correlation matrix of a potential failure dataset. As previously mentioned, a new correlation matrix is calculated based on the measurement points after the threshold is exceeded.

The sampling distribution of the healthy and faulty correlation coefficient matrices does not follow a normal distribution. Fisher r-to-z transformation is used to convert these data sets into a normally distributed variable z. This transformation is made as follows:

$$z_r = \frac{1}{2} log\left(\frac{1+r}{1-r}\right) \quad (10)$$

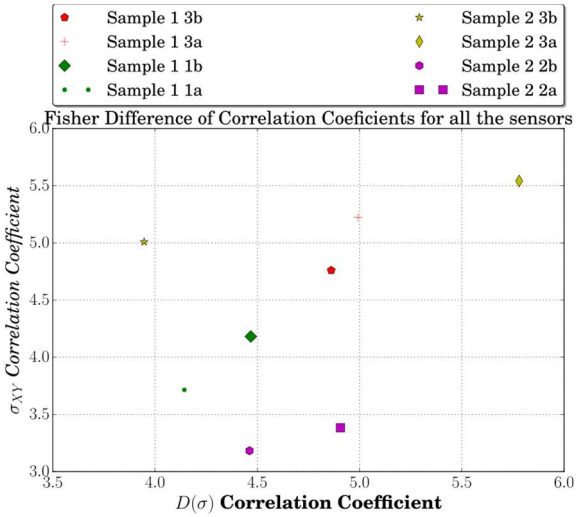

Figure 16. Fisher Correlation Coefficient Difference. This difference is performed by using Fisher method of comparing two correlation coefficients. In this case all the sensors correlation coefficient data have been compared with the correlation coefficient as healthy state. The values from the graph represents the z-score values.

This transformation is performed at a confidence value interval of 0.95. Each correlation coefficient parameter in the data is compared with the correspondent one and then a mean is performed on the stress difference and shear stress performance parameters.

Plotting them against each other is depicted in Figure 16. From this graph it is concluded that some sensor data is more damaged than the others. The most damaged one is showed in yellow representing the Sample 3 sensor 3a. From Figure 7 it is observed that the outer molding compound is delaminated from the package of sensor 3a.

3) Feature Extraction

PCA is used to identify patterns in data and to express the data to highlight their similarities and differences [15]. Also, this last step is performed to reduce the data as much as possible, to understand the data much better and to make the classification much easier to be performed.

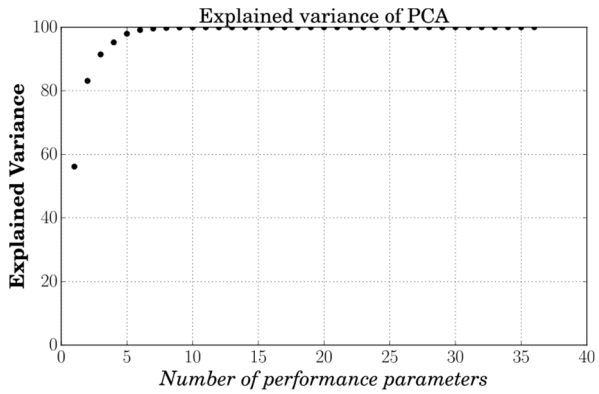

Figure 17. Explained variance.

The PCA analysis is performed on the data matrix and the explained variance is extract as shown in Figure 17. Only the principal components exceeding 97% of the variance are kept. Therefore only 6 principal components are left to perform PCA analysis and the extracted results of each performance parameter influence on the principal components is shown in TABLE I. It is observed that the weight of each parameter reveals that the first component takes the most influence from stress difference performance parameters and the second component takes the effect from shear stress performance parameters. Plotting first and second component as in Figure 18 it is observed the influence of stress difference and shear stress in the delamination process. Again as previously observed, the yellow markers representing sensor 3 from Sample 2 is situated as the most damaged one.

The sensor symmetry is identified from Figure 18 and Figure 19. The behavior of the sensors in both figures is quite similar, but with opposite sign. Considering this property, a classification strategy can be implemented, considering the data from one sensor as training data and the data from the other sensor as validation.

Briefly a PCA is performed as follows:

- Step 1. Subtract the mean

$$\bar{x}_i = \frac{1}{m}\sum_{j=1}^{m} x_{ij} \qquad (11)$$

- Step 2. Calculate the covariance matrix

$$cov(x_i, x_j) = \frac{\sum_{i,j}^{n}(x_i - \bar{x})(x_j - \bar{x})}{n-1} \qquad (12)$$

- Step 3. Calculate the eigenvectors and eigenvalues of the covariance matrix
- Step 4. Choosing the eigenvectors with the highest eigenvalue
- Step 5. Reconstructing the data matrix with the new set of parameters

TABLE I. PCA REDUCED PARAMETERS

	PCA reduced parameters					
	1	*2*	*3*	*4*	*5*	*6*
D(σ)	**0.203**	0.032	0.039	0.085	-0.045	**-0.203**
	0.209	-0.019	-0.086	0.070	-0.064	-0.065
	0.174	-0.110	-0.160	0.001	0.057	0.163
	0.213	-0.010	-0.093	0.029	-0.039	0.026
	0.213	0.051	0.014	-0.021	-0.016	-0.049
	0.189	0.092	0.136	-0.094	-0.036	-0.090
	0.173	0.125	0.154	-0.130	0.038	-0.034
	0.209	0.059	0.061	-0.083	0.008	0.009
	0.212	-0.039	-0.031	0.072	-0.004	0.087
	0.191	-0.090	-0.074	-0.009	0.030	**0.220**
	0.208	-0.037	-0.066	-0.050	0.011	0.097
	0.200	0.065	0.079	-0.107	0.049	0.058
σ_{xy}	-0.039	**0.247**	0.128	-0.107	0.054	0.088
	-0.031	**0.257**	0.102	0.041	0.023	-0.088
	-0.009	**0.259**	0.085	0.095	-0.006	-0.039
	-0.039	**0.245**	0.117	-0.027	0.145	-0.127
	-0.021	**0.257**	0.123	0.003	-0.053	0.089
	-0.022	**0.256**	0.019	-0.162	-0.039	0.054
	0.069	0.179	0.110	**0.270**	-0.230	0.164
	-0.043	**0.249**	-0.134	0.013	0.015	0.045
	-0.006	**0.252**	-0.080	-0.150	0.084	0.014
	-0.117	**0.198**	-0.180	-0.003	0.087	-0.001
	-0.153	0.008	-0.203	0.183	**0.255**	-0.111
	0.043	**0.154**	-0.319	-0.096	0.066	-0.139

With the data reduced to 6 performance parameters, it can be furthered used for transmitting the data. The transmitted data can be reconstructed in the initial number of parameters or it can be used as it is. The classification methods can use both datasets.

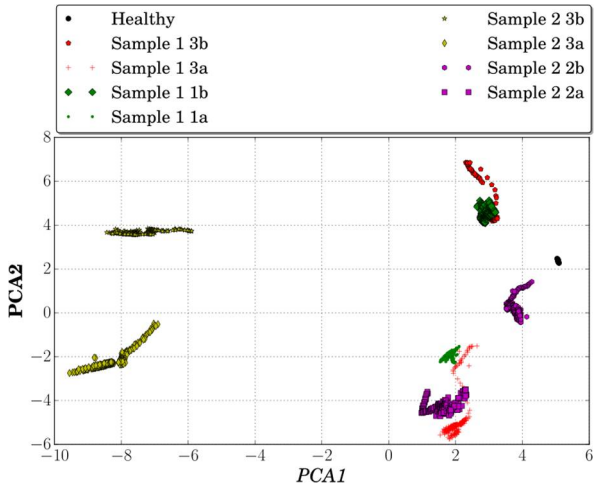

Figure 18. Principal components influence over the delamination areas.

In Figure 18 the most dominant principal components are depicted, reducing the high dimension of the data to these 2 components makes it easier to understand the global influence of different delamination areas on the stress difference and shear stress components.

As expected the sensor 3a and 3b data from Sample 2 shows the biggest distance from the healthy baseline at least in the first component axis, which is represented in most part by stress difference component.

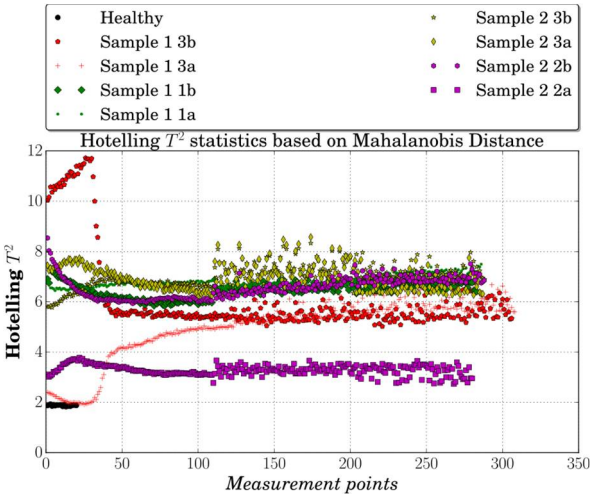

Figure 19. Hoteling T2 statistics in the reduced space at room temperature during delamination. The red line corresponding to the same sensor but mirrored can identify a similar behavior, but opposite sign.

Based on the reduced space Hoteling T2 statistics is performed and is depicted in Figure 19. In this graph is observed as well that the stresses reach a high peak and then there is a drop, which confirms our previous observations that before the delamination there is an increase in the stress state followed by a drop representing the physical delamination.

V. Conclusions and Future Work

It has been demonstrated that the piezoresistive silicon based stress sensor is capable of detecting and quantifying delamination. Also, the resulting data shows the symmetry of the sensors. The algorithms applied to the sensor data revealed valuable information that can be furthered studied.

Further research studies will be performed on the importance of the new parameters and their connection to the failure, the slope registered at the temperature cycling during delamination, classification methods applied to principal components and the possibility to build a prognostic model based on the damage quantification parameter.

The ultimate goal is to develop and implement PHM for various application requirements. Usually these requirements are projected into a PHM Framework. There are many PHM frameworks proposed in the literature for different applications [18][20]. The principles are in general the same for most of them, but for each particular application PHM frameworks must be modified and optimized for specific requirements.

In the present case of ECU application, it is desired to have certain calculations and data processing inside the acquisition system as depicted in Figure 20. In this paper the first part of this framework was presented, which is the data acquisition, data manipulation, health assessment and damage quantification. The second part of the frame work will be reported in the future publication.

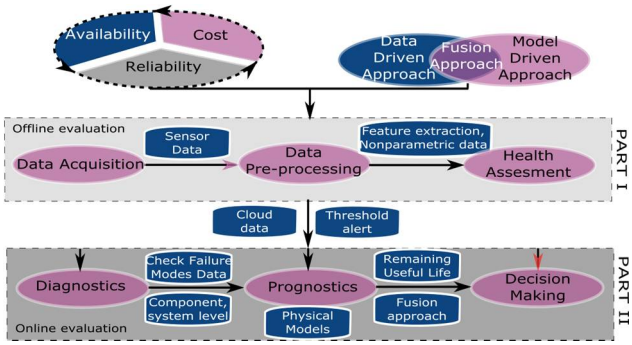

Figure 20. Prognostics and Health Monitoring framework. In this paper it is presented the process of acquiring, processing and asses the stress data as being Part I. Offline evaluation in this context means that the process is performed inside the acquisition unit.

References

[1] J. C. Suhling, R. C. Jaeger, and others, "Silicon piezoresistive stress sensors and their application in electronic packaging," *IEEE Sens. J.*, vol. 1, no. 1, pp. 14–30, 2001.

[2] P. Gromala *et al.*, "Internal stress state measurements of the large molded electronic control units," in *Thermal, Mechanical and Multi-Physics Simulation and Experiments in Microelectronics and Microsystems (EuroSimE), 2013 14th International Conference on*, 2013, pp. 1–8.

[3] T. Schreier-Alt, K. Unterhofer, F. Ansorge, and K.-D. Lang, "Stress analysis during assembly and packaging," in *Electronic Components and Technology Conference (ECTC), 2011 IEEE 61st*, 2011, pp. 1684–1690.

[4] A. R. R. Adli and K. M. B. Jansen, "Numerical investigation and experimental validation of residual stresses building up in microelectronics packaging," *Microelectron. Reliab.*, vol. 62, pp. 26–38, Jul. 2016.

[5] T. Schreier-Alt, G. Chmiel, F. Ansorge, and K.-D. Lang, "Piezoresistive stress sensor for inline monitoring during assembly and packaging of QFN," in *2013 IEEE 63rd Electronic Components and Technology Conference*, 2013, pp. 2126–2131.

[6] F. Schindler-Saefkow *et al.*, "Measuring the mechanical relevant shrinkage during in-mold and post-mold cure with the stress chip," in *Thermal, mechanical and multi-physics simulation and experiments in microelectronics and microsystems (eurosime), 2014 15th international conference on*, 2014, pp. 1–5.

[7] Y. Kim, H. Lee, S. Park, and X. Zhang, "Stress relaxation test of molding compound for MEMS packaging," in *Thermal and Thermomechanical Phenomena in Electronic Systems (ITherm), 2012 13th IEEE Intersociety Conference on*, 2012, pp. 290–296.

[8] A. Palczynska, P. J. Gromala, D. Mayer, B. Han, and T. Melz, "In-situ investigation of EMC relaxation behavior using piezoresistive stress sensor," *Microelectron. Reliab.*, vol. 62, pp. 58–62, 2016.

[9] A. Palczynska, A. Prisacaru, P. J. Gromala, B. Han, D. Mayer, and T. Melz, "Towards prognostics and health monitoring: The potential of fault detection by piezoresistive silicon stress sensor," in *2016 17th International Conference on Thermal, Mechanical and Multi-Physics Simulation and Experiments in Microelectronics and Microsystems (EuroSimE)*, 2016, pp. 1–8.

[10] B. Wu, D.-S. Kim, B. Han, A. Palczynska, and P. J. Gromala, "Thermal deformation analysis of automotive electronic control units subjected to passive and active thermal conditions," in *Thermal, Mechanical and Multi-Physics Simulation and Experiments in Microelectronics and Microsystems (EuroSimE), 2015 16th International Conference on*, 2015, pp. 1–6.

[11] M. K. Rahim, J. Roberts, J. C. Suhling, R. C. Jaeger, and P. Lall, "Continuous In-Situ Die Stress Measurements During Thermal Cycling Accelerated Life Testing," in *2007 Electronic Components and Technology Conference*.

[12] A. Palczynska, F. Pesth, P. J. Gromala, T. Melz, and D. Mayer, “Acquisition unit for in-situ stress measurements in smart electronic systems,” in *Thermal, mechanical and multi-physics simulation and experiments in microelectronics and microsystems (eurosime), 2014 15th international conference on*, 2014, pp. 1–4.

[13] S. Kumar, V. Sotiris, and M. Pecht, “Mahalanobis Distance and Projection Pursuit Analysis for Health Assessment of Electronic Systems,” in *2008 IEEE Aerospace Conference*, 2008, pp. 1–9.

[14] R. A. Fisher, “Biological Monographs And Manuals Vol-5,” 1934.

[15] H. Anton, *Elementary linear algebra*. New York: Wiley, 1987.

[16] D.-S. Kim, B. Han, A. Yadur, and P. J. Gromala, “Electronic control package model calibration using moiré interferometry,” in *Thermal, mechanical and multi-physics simulation and experiments in microelectronics and microsystems (eurosime), 2014 15th international conference on*, 2014, pp. 1–5.

[17] A. Palczynska *et al.*, “Investigation of Uncertainty Sources of Piezoresistive Silicon Based Stress Sensor,” *Appl. Mech. Mater.*, vol. 807, pp. 45–54, 2015.

[18] M. Pecht, “Prognostics and Health Monitoring of Electronics,” in *International Conference on Electronic Materials and Packaging, 2006. EMAP 2006*, 2006, pp. 1–10.

[19] S. Kumar, T. W. S. Chow, and M. Pecht, “Approach to Fault Identification for Electronic Products Using Mahalanobis Distance,” *IEEE Trans. Instrum. Meas.*, vol. 59, no. 8, pp. 2055–2064, Aug. 2010.

[20] P. Lall, P. Gupta, D. Panchagade, M. Kulkarni, J. Suhling, and J. Hofmeister, “Prognostics and condition monitoring of electronics,” in *Thermal, Mechanical and Multi-Physics simulation and Experiments in Microelectronics and Microsystems, 2009. EuroSimE 2009. 10th International Conference on*, 2009, pp. 1–14.